Crystal plasticity modeling the deformation in nanodomained heterogeneous structures

Tianju Chen¹, Caizhi Zhou^{1,2,*}

¹ Department of Materials Science and Engineering, Missouri University of Science and

Technology, Rolla, MO 65409, USA

² Department of Mechanical and Aerospace Engineering, Missouri University of Science and

Technology, Rolla, MO 65409, USA

Abstract

Nanodomained heterogeneous structures characterized by randomly dispersed nano grains (NGs)

embedded in the coarser grains (CGs) have demonstrated an exciting potential to break the

strength-ductility trade-off, providing high strength without the loss of ductility. Here, using a

combination of discrete crystal plasticity finite element (discrete-CPFE) model and dislocation

density-based CPFE model, we study the effects of grain size, volume fraction of nano grians on

the strength and deformation in nanodomained materials. Our analysis shows that the overall

flow stresses of nanodomained samples are equal or higher than the strengths predicted by rule

of mixtures (ROM). Smaller NGs or higher volume fraction of NGs can make the nanodomained

samples stronger, as they can be more effective to promote the dislocation accumulations inside

the CGs and eventually raise the CRSS for each slip system during the plastic flow. Areas

surrounding NGs stored higher dislocation densities and less plastic strain, due to the restricted

dislocation motion. Furthermore, NGs grain embedded in the CGs can effectively reduce the

anisotropy of strength in the nanodomained samples.

Key words: Nanodomain; Grain size; Crystal plasticity; Nanocrystalline; Finite element model

* Corresponding author.

1. Introduction

Over the past 30 years of research shows that the nanocrystalline (NC) materials usually have high strength and hardness. Without changing the material chemical composition, the strength and hardness of NC materials can be several times or even dozens of times as that to the same component of coarse grain (CG) materials ¹⁻⁶. However, with the significant increment of strength and hardness, the plasticity and toughness of NC materials drops substantially, and work hardening ability disappears. The structural instability and the performance deterioration restrict the performance and applications of NC materials.

With the process of new nanotechnologies, building nano-structures into architecture can effectively overcome the drawback of NC materials at the same time giving full play to the advantages of their performance. There are several examples for the architectured NC materials, such as the gradient nanograined structure 1-6, heterogeneous lamella structure 7-10, bimodal structure ^{8, 11-13}, and nanodomained structure ¹⁴. These materials have a common feature that a remarkable difference in the strength between different domains, while the sizes and shape of the domains may vary significantly. The gradient nano structure refers to the structure of the unit size (such as grain size or the layer thickness on the space gradient change, from the nanoscale continuous increase to macro scale. The essence of gradient nano-structure is that the density of grain boundary (or other interfaces) changes by gradient in space, so it corresponds to the gradient change of many physical or chemical properties in space. Lu et al. claimed that in gradient nanocrystals, the plastic deformation takes place in a chain-like manner, that is, the core of the coarse-grain first plastically deforms, and then the plastic deformation gradually passes from the coarse-grain region to the surface nanocrystalline region. In that way, the strain hardening of the core and the stress-induced growth of the surface nanocrystals can be obtained,

so the chain plastic deformation can effectively inhibit premature necking ². Different from the gradient structures, the heterogeneous lamella structure is characterized with alternating lamellae of soft micro/macro grains and hard nano/ultrafine grains, and can be fabricated by accumulative roll bonding process and subsequent annealing ¹⁰. The heterogeneities of grain size, hardness and texture across the interfaces can simultaneously improve the strength and ductility of the whole structures. While the bimodal structure can be obtained by a combination of cryogenic rolling and subsequently recrystallization process, and contains a bimodal distribution of grain size with micro grains randomly embedded into nano/ultrafine grains. The bimodal structured materials possess a high strain hardening rate, like the coarse grained materials. The additional work hardening ability of heterogeneous lamella structure and bimodal structure results from the accumulation of dislocations due to the large number of geometrically necessary dislocation formed across the boundary between micro grains and nano/ultrafine grains ⁷.

Motivated by the bimodal structures, Wu et al. ¹⁴ processed a new class of nanostructured materials, nanodomained materials, via a pulsed electroplating protocol. These nanodomained materials are characterized by randomly dispersed nano grains embedded in the coarser grains (CG). Even with 2.5% embedded nano grains, the yield strength of the nanodomained materials is comparable to the pure NC materials, while the high strain hardening rate and good ductility are realized simultaneously. During the deformation of nanodomained materials, the nano grains act like precipitates which can block the dislocation motion, in the meanwhile, boundaries around the nano grains can absorb and emit dislocations. That can balance the dislocation storage and multiplication rates and result in the exceptional strain hardening capacity to maintain the large uniform deformation. However, several critical questions are still unanswered for the development of ductile high strength nanodomained

materials: i) how do the volume fraction and grain sizes of nano grains control the strain hardening behavior of the whole structure? ii) how do the orientations of the coarse grains affect the dislocation accumulation in the nanodomained structure? iii) What is the mechanism by which nanodomained materials retain their ductility and how can we enhance this effect?

Through the development of computer resources, various modeling tools are available for exploring the mechanical behavior of materials to provide the guideline for materials design. Molecular dynamics simulations are able to reveal single or a few defects activities during deformation, but is limited by the time-scale and length-scale ^{15, 16}. Classic crystal plasticity finite element (CPFE) modeling can predict the mechanical behavior of micro-scale materials as the dislocation motion and interactions in phases dominate the deformation processes ¹⁷. However, most CPFE models either use phenomenological constitutive formulations to describe dislocation-induced property evolution, such as strain hardening, or treat dislocations in a homogenized and statistical manner. They are lack of GBs physics, such as dislocation nucleation, motion, reactions with GBs.

In this study, we combine a novel discrete crystal plasticity finite element (discrete-CPFE) model with dislocation density-based CPFE model to study the effects of grain size, volume fraction of nano grians on the strength and deformation in nanodomained materials. We also explore the influence of coarse grain orientations on the dislocation accumulation and strain distribution within the nanodomained structure.

2. Methodology

A rate-dependent elasto-viscoplastic constitutive model accounting for elastic and plastic deformation of crystals and the underlying kinematic relations developed by Marin et al. ¹⁸ is

modified to accommodate the discrete CPFE model used in this work. The \mathbf{L}^p is the plastic velocity gradient is calculated by:

$$\mathbf{L}^{\mathbf{p}} = \sum_{\alpha=1}^{N} \dot{\mathbf{y}}^{\alpha} \mathbf{s}^{\alpha} \otimes \mathbf{m}^{\alpha} \tag{1}$$

where N is total number of slip systems in a single crystal, $\dot{\gamma}^{\alpha}$ is the shear strain rate of slip system α , s^{α} and m^{α} are the slip direction and slip plane normal of slip system α , respectively, and $s^{\alpha} \otimes m^{\alpha}$ defines the Schmid tensor.

The corresponding shear strain rate in slip system α is calculated with a power-law equation:

$$\dot{\gamma}^{\alpha} = \dot{\gamma}_0 \left[\frac{|\tau^{\alpha}|}{\tau_{CRSS}^{\alpha}} \right]^{\frac{1}{m}} sign(\tau^{\alpha}) \tag{2}$$

where $\dot{\gamma}_0$ is a reference shear strain rate, τ^{α} and τ^{α}_{CRSS} are resolved shear stress (RSS) and critical resolved shear stress (CRSS) in slip system α , respectively, and m is the strain rate sensitivity exponent.

In this study, we use two different models to evaluate the CRSS in NGs and CGs as their deformation mechanisms are different from each other. In NGs, we adopt a novel grain boundary discrete slip model to calculate the CRSS ^{19, 20}, since the conventional crystal plasticity model cannot capture the deformation physics in NGs. In the grain boundary discrete slip model, the plastic strain within nano grains is assumed to be induced by the slip of dislocations nucleated from the GBs. The CRSS is controlled by the length of GB dislocations, and equals to the stress required for activating the GB dislocation and subsequently gliding across the grain. Since the GB structure varies with the GB types and local misorientations, the length of the GB dislocation

is not uniform, but follows a normal distribution as shown in Figure 1 (a). The upper and lower limits of the length of GB dislocations are the dislocation core size and the grain size, respectively. The dislocation source distribution can be converted to the CRSS distribution via Foreman's formula ²¹

$$\tau_{CRSS}^{\alpha} = \frac{\mu b}{2\pi L} \log\left(\frac{L}{r_0}\right) \tag{3}$$

where, μ is the shear modulus of the metal, b is the magnitude of Burgers vector, L is dislocation source length, and r_0 is dislocation core size, which is set as 2b. The CRSS distribution follows the generalized extreme value distribution (Figure 1 (b)) that will be used in our work to calculate the shear strain rate in each slip system.

For the CG part, we employ a dislocation density based model to evaluate the CRSS during the plastic deformation, as the dislocation motion and reactions dominate the plastic deformation in CGs. The CRSS is calculated based on the following formula:

$$\tau_{CRSS}^{\alpha} = \chi G b \sqrt{\rho_{SSD}^{\alpha} + \rho_{GND}^{\alpha}} + \tau_{Sub}^{\alpha} + \tau_{GB} \tag{4}$$

where χ is the dislocation interaction factor and ρ_{SSD}^{α} and ρ_{GND}^{α} are statistically stored dislocation (SSD) and geometrically necessary dislocation (GND) density in slip system α , respectively. τ_{Sub}^{α} is the resistance for the dislocation motion contributed from dislocation substructures ²². τ_{GB} is the dislocation motion resistance arising from grain boundaries ²³.

The SSD density evolves with strain and varies with dislocation trapping and annihilation rates ²⁴, and is governed by

$$\frac{\partial \rho_{SSD}^{\alpha}}{\partial \gamma} = \frac{\partial \rho_{gen,SSD}^{\alpha}}{\partial \gamma} - \frac{\partial \rho_{rec,SSD}^{\alpha}}{\partial \gamma} = k_1 \sqrt{\rho_{SSD}^{\alpha}} - k_2 (\dot{\varepsilon}, T) \rho_{SSD}^{\alpha}$$
 (5)

where $\rho_{gen,SSD}^{\alpha}$ is the trapped SSD density and $\rho_{rec,SSD}^{\alpha}$ is the recovered part in slip system α , respectively. The parameter k_1 is a coefficient for statistical trapping of mobile dislocations and k_2 is a coefficient for annihilation of trapped dislocations. The latter is a function of temperature and strain rate and related to k_1 via:

$$\frac{k_2}{k_1} = \frac{\chi b}{g} \left(1 - \frac{kT}{\tau_D b^3} \ln \left(\frac{\dot{\varepsilon}}{\dot{r}} \right) \right) \tag{6}$$

where k is the Boltzmann constant, g is an effective activation enthalpy, T is the temperature, τ_D is a drag stress, $\dot{\varepsilon}$ is the applied strain rate and \dot{r} is a characteristic rate that is related to the number of attempts to overcome barriers to slip.

The evolution of the GND density is calculated by the formula derived by Ma et al. 25

$$\dot{\rho}_{GNDS}^{\alpha} = \frac{1}{h} \| \nabla_{\mathbf{x}} \times (\dot{\gamma}^{\alpha} \mathbf{F}_{P}^{T} \mathbf{n}^{\alpha}) \| \tag{7}$$

where the nabla operator $\nabla_{\mathbf{x}}$ is defined as the derivative with respect to the reference coordinate, and \mathbf{F}_P is the irreversible plastic strain. During the calculation, $\dot{\rho}_{GND}^{\alpha}$, is decomposed into three groups: one group of screw dislocations with tangent vector parallel to the slip direction, \mathbf{d}^{α} , the other two groups of edge dislocations with tangent vectors parallel to \mathbf{n}^{α} and \mathbf{t}^{α} , respectively, and can be obtained by:

$$\dot{\rho}_{GNDS}^{\alpha} = 1/b[\nabla_{\mathbf{x}} \times (\dot{\gamma}^{\alpha} \mathbf{F}_{P}^{T} \mathbf{n}^{\alpha})] \cdot \mathbf{d}^{\alpha}$$
(8)

$$\dot{\rho}_{GNDet}^{\alpha} = 1/b[\nabla_{\mathbf{x}} \times (\dot{\gamma}^{\alpha} \mathbf{F}_{P}^{T} \mathbf{n}^{\alpha})] \cdot \mathbf{t}^{\alpha}$$
(9)

$$\dot{\rho}_{GNDen}^{\alpha} = 1/b \left[\nabla_{\mathbf{x}} \times (\dot{\gamma}^{\alpha} \mathbf{F}_{P}^{T} \mathbf{n}^{\alpha}) \right] \cdot \mathbf{n}^{\alpha}$$
 (10)

Finally, the change of GND density, $\dot{\rho}^{\alpha}_{\text{GND}}$ is calculated by:

$$(\dot{\rho}_{GND}^{\alpha})^{2} = (\dot{\rho}_{GNDS}^{\alpha})^{2} + (\dot{\rho}_{GNDet}^{\alpha})^{2} + (\dot{\rho}_{GNDen}^{\alpha})^{2}$$
(11)

The second term in the CRSS equation (4) is the contribution from substructure dislocation densities, and can be express according to the extended Taylor laws ²²:

$$\tau_{sub}^{\alpha} = k_{sub} \mu b \sqrt{\rho_{sub}^{\alpha}} \log \left(\frac{1}{b \sqrt{\rho_{sub}^{\alpha}}} \right)$$
 (12)

where k_{sub} is a mathematical constant for recovering the Taylor law when substructure dislocation densities is at relatively low level.

And the evolution of substructure density is dependent on the recovery rate ²⁶:

$$\Delta \rho_{sub}^{\alpha} = qb \sqrt{\rho_{sub}^{\alpha}} k_2 \rho_{for}^{\alpha} \sum_{\alpha} |\Delta \gamma^{\alpha}|$$
(13)

where q is a temperature-dependent rate coefficient ²⁶

$$q = q_0 \ln \left(1 + \frac{T}{q_1} \right) \tag{14}$$

The preceding constitutive formulations are written as a user-defined material (UMAT) subroutine and implemented in finite element software package Abaqus CAE. To validate our model, we performed our calculations for NC Ni and CG Ni separately. The parameters and initial values of densities for different type of dislocations used in our calculations are listed in Table 1. The predicted stress-strain curves compared with the experiment curves from different research groups are shown in Figure 1 (c). The experiment data for NC Ni 27,28 and CG Ni 29 are used to validate our discrete-CPFE model and the dislocation density-based model, respectively. It is worth to mention that the values for χ , k_1 , g and τ_D are simply to acquire the best fit with the experiment stress-strain curves for CG Ni, while the values for other parameters are obtained from the reference²⁶. From Figure 1(c), we can see our predicted results match well with the

experiment curves, such as the yield strength, flow strength and strain hardening behavior. In addition, our model also accurately predicts the grain size effect on the strength of NC Ni. Here, we want to point out that the tiny mismatch between the predicted and experimental curves, especially for 20nm NGs, is mainly induced by the difference on the grain size in experimental samples and our model. In our model, we assume all grains possess the same grain size equal to the average grain size measured from experimental studies, while the grain size of each grain in experimental samples may be different from the average grain size and vary with each other.

Table 1 Parameters in the dislocation density based model for CG Ni

$C_{11} (GPa)^{30}$	C ₁₂ (GPa) ³⁰	C ₄₄ (GPa) ³⁰	μ (GPa) ¹⁹	b (nm) 19	$\dot{\gamma}_0$ (s ⁻¹)	m
246.5	147.3	124.7	76	0.25	0.01	0.1
χ	$k_1 (\text{m}^{-1})$	g	<i>T</i> (K)	τ_D (MPa)	\dot{r} (s ⁻¹) ³⁰	
0.3	1.13×10 ⁹	2.7×10 ⁻²	298	900	1×10 ⁷	
q_0^{30}	$q_1(K)^{30}$	$k_{sub}30$	$\rho_{SSD}^{\alpha}(\text{m}^{-2})$	$\rho_{GND}^{\alpha}(\text{m}^{-2})$	$\rho_{sub}^{\alpha}(m^{-2})$	
47.22	800.0	0.086	5×10^{12}	0	5×10^{1}	

In order to identify the role of nano grains on the deformation of the nanodomained structure, we create the FE mesh with 8000 (20×20×20) elements to mimic one coarse grain as shown in Figure 2, in which nano grains are randomly embedded. Since the volume fraction of the 7 nm nano grains in the experiment studies is about 2.5% ¹⁴, we use two different volume fractions 1% and 2.5% in this study to reveal the influence the volume fraction of the nano grains on the strength of nanodomained Ni. In addition, the nano grains size will be changed from 7 nm to 50 nm to understand how the nano grain size affect the deformation in nanodomained Ni. Furthermore, three different orientations ([001], [111] and [123]) are used in this work for the coarse grain. [001] and [111] orientations are two typical multiple-slip orientations which have

multiple slip systems possess the maximum Schmid factor as the same time, while [123] orientation is single-slip orientation with only one slip system holding the maximum Schmid factor. For nano grains, we randomly assign a crystallographic orientation to each grain in this work. The position of each nano grain in the mesh is fixed and the orientation of each nano grain does not change from one case to another. Thus, the influence of the spatial variation of the nano grains on the calculated results will be excluded.

To model the strengthening effect of nano grains in bulk coarse grains, periodic boundary conditions have been applied in all three directions and the uniaxial tension is applied along the X direction at a constant strain rate, $\dot{\varepsilon} = 1 \times 10^{-4} s^{-1}$. Based on the periodic boundary condition provided by Choi et al. ³¹, the displacements of two equivalent nodes (a) and (b) on opposite sides of the mesh are coupled with the deformation gradient, \bar{F}_{ij} :

$$u_i^a - u_i^b = \bar{F}_{ij}(x_{j0}^a - x_{j0}^b) - (x_{i0}^a - x_{i0}^b)$$
(15)

where x_{i0}^a and x_{i0}^b represent the coordinates of the paired nodes in the pre-deformed configuration. This boundary condition can minimize the constraint effect and make the quantitative comparison of results from cases with different volume fractions and grains sizes more accurate.

3. Results and discussion

Figure 3 shows the calculated stress-strain curves of the nanodomained samples for different cases. For two different volume fractions (1.0% and 2.5%), the samples with [111] orientated coarse grains always exhibit the highest strengths, as the average Schmid factor of 12 slip systems in the [111] orientated grains is 0.136 and smaller than 0.272 for the [001] orientated and 0.185 for [123] orientated grains. Normally, lower Schmid factors result in smaller RSS for

the corresponding slip systems, which cannot activate the slip events or can only generate low shear strain rates. Thus, higher applied stresses are needed to activate more slip events or bump up the shear strain rates to satisfy the external imposed strain. This is why the samples with [111] and [001] coarse grains show the highest and lowest strengths, respectively.

In addition, it is clear that the smaller size of nano grains or larger volume fraction of nano grains can make the nanodomained samples stronger, as the sample with 7 nm NGs are possess higher strength than the sample with 50 nm NGs at the same volume fraction, and the samples with 2.5% NGs exhibit enhanced strengths compared to samples with 1.0% NGs. In order to check whether the strength of the nanodomained samples follow the rule of mixtures, in Figure 3, we also compare the CPFE predicted stress-strain curves with the results predicted by rule of mixtures (ROM), $\sigma_{ROM} = \sum V_i \sigma_i$, where V_i is the volume fraction and σ_i is the strength of each single phase ³². ROM always predicts the upper limit of the strength of composites, especially for the composites only under elastic deformation, as the ROM was derived based on the isostrain condition that assumes each phase within the composite sustains the same amount of strain. From figure 3, we can see that the CPFE predicted stress-strain curves are below the ROM curves at the beginning of the deformation with the total strain smaller than 0.02, although the overall flow stresses of nanodomained samples are equal or higher than the strengths predicted by ROM for different volume fraction and NG sizes. For the small strain region, both the CGs and NGs were under elastic deformation or plastically deformed a small amount. As the NGs in the nanodomained samples were not perfectly aligned with the CG under isostrain condition but randomly distributed within the CG, it is not surprising to see the ROM predicted strengths are higher than the strengths of nanodomained samples. As the difference on the strength between the 50 nm NGs and CGs is smaller than that between 7 nm NGs and CGs, the stress-strain curves

for nanodomained Ni with 50 nm NGs are close to the ROM curves at the beginning of the deformation. When the nanodomained samples were deformed to large strains, their strengths have caught up with or surpassed the ROM strengths as shown in Figure 3.

In the coarse grained metals, the strain hardening behavior, i.e. the flow stress increases with the strain during the plastic deformation, is controlled by the dislocation motion, multiplication and interactions. Higher dislocation density is more effective on restricting the dislocation motion that results in less plastic strain and higher flow stress under the same amount of deformation. Thus, we plot the dislocation density over the strain for different cases in Figure 4. It is clear that the dislocation densities in all nanodomained samples are much higher than those for the corresponding pure CG samples. Furthermore, the samples with [111] and [001] orientated CGs carry the highest and lowest dislocation densities, while the dislocation densities in samples with [123] CGs are between those two cases. In addition, the dislocation densities in samples with 7 nm NGs are higher than those in in samples with 50 nm NGs. Raising the volume fraction of NGs from 1% to 2.5% induced larger difference on the dislocation density 7 nm sample than that 50 nm samples.

To reveal the role of the dislocation density on the plastic deformation in nanodomained samples, we output the distribution of the dislocation density and equivalent plastic strain distributions in Figure 5. Based on our model, we assume there is no dislocation accumulation within the NGs, which is consistent with most experiment results from the heavily deformed nanocrarylline metals ³³ and also supported by atomistic simulation results^{34,35}. In Figure 5, the coarse grain elements surrounding NGs always possess high dislocation densities. The NGs embedded in the CG serves a dual role during the plastic deformation. As the strength of NGs is very high compared to the corresponding CGs, they can strength the whole nanodomained

sample as hard particles. Secondly, the NGs can effective block the pathway for dislocation motion that results in high accumulative dislocations inside the CGs. In addition, large mismatch of strengths between the NGs and CGs can also induce high GND density from the plastic strain gradients during the plastic flow. In Figure 5, we also plot the distribution of the equivalent plastic strain in the nanodomained sample with 2.5% 7 nm NGs. We can see that the distribution of equivalent plastic strain in the nanodomained sample is highly heterogeneous. The elements surrounding NGs exhibit less equivalent plastic strain than those far from the NGs, which resulted from the restricted dislocation motion within those elements.

In polycrystalline metals, the anisotropy on some important properties, such as yield strength and ductility, often results from their preferred crystallographic orientation. The anisotropy of strength in single crystalline materials is usually caused by the Schmid factors that are determined by the angles between the loading direction and slip systems. Beside the Schmid factor effect, the dislocation structures and densities can also play an important role on the anisotropy of strength³⁶⁻³⁸. Since NGs bring on the change of total dislocation density in the CGs during plastic deformation, it raises an important question: how does the embedded NGs affect the anisotropy of strength? Thus, we compared the difference on the flow stress at 0.1 strain between the samples with [001] CG and [111], [123] CGs in Figure 6. We can see that the difference on the flow stress between samples with [111] CG and [001] CG is always larger than the difference between [123] CG and [001] CG, as the average Schmid factors for [111] and [001] CGs are the highest and lowest among those three cases. In addition, our results indicate the embedded NGs can relieve the anisotropy of strength in the nanodomained samples, as the nanodomained samples display smaller differences between different orientations than those in CG samples. Furthermore, smaller NGs and high volume fraction of NGs are more effective on

reducing the anisotropy of strength. That is because smaller NGs and high volume fraction of NGs can raise the dislocation density inside the CGs as shown in Figure 4. That can efficiently stop or slow down the dislocation motion, and make the value of CRSS for different slip systems close to each other, and consequently alleviate the anisotropy of strength.

4. Conclusions

In this work, we studied the effects of grain size, volume fraction of nano grians on the strength and deformation in nanodomained materials by using a combination of discrete-CPFE model and dislocation density-based CPFE model. Our analyses reveal that the overall flow stresses of nanodomained samples are equal or higher than the strengths predicted by ROM. In addition, smaller NGs or higher volume fraction of NGs can make the nanodomained samples stronger, as they can be more effective to promote the dislocation accumulations inside the CGs and eventually raise the CRSS for each slip system during the plastic flow. Areas surrounding NGs possess higher dislocation densities and less plastic strain, as the dislocation motion was restricted. Furthermore, NGs grain embedded in the CGs can reduce the anisotropy of strength of the nanodomained samples. These findings shed light on the role of NGs in the plastic deformation of nanodomained metals and can benefit he design and processing of ultrahigh strength ductile heterogeneous nanostructured metals.

Acknowledgements

This work was supported by NSF CAREER Award (CMMI-1652662). C.Z. also acknowledges support by the Extreme Science and Engineering Discovery Environment (XSEDE), award number DMR170093.

References

- 1. K. Lu: Making strong nanomaterials ductile with gradients: Microstructures that increase metal crystallite size from nanoscale with surface depth are both strong and ductile *Science*. **345**(6203), 1455 (2014).
- 2. T.H. Fang, W.L. Li, N.R. Tao and K. Lu: Revealing extraordinary intrinsic tensile plasticity in gradient nano-grained copper *Science*. **331**(6024), 1587 (2011).
- 3. X. Wu, P. Jiang, L. Chen, F. Yuan and Y.T. Zhu: Extraordinary strain hardening by gradient structure *Proceedings of the National Academy of Sciences of the United States of America.* **111**(20), 7197 (2014).
- 4. X.L. Wu, P. Jiang, L. Chen, J.F. Zhang, F.P. Yuan and Y.T. Zhu: Synergetic strengthening by gradient structure *Mater. Res. Lett.* **2**(4), 185 (2014).
- 5. A. Chen, J. Liu, H. Wang, J. Lu and Y.M. Wang: Gradient twinned 304 stainless steels for high strength and high ductility *Materials Science and Engineering: A.* **667**, 179 (2016).
- 6. Y. Wei, Y. Li, L. Zhu, Y. Liu, X. Lei, G. Wang, Y. Wu, Z. Mi, J. Liu, H. Wang and H. Gao: Evading the strength-ductility trade-off dilemma in steel through gradient hierarchical nanotwins *Nature Communications*. 5, (2014).
- 7. X. Wu, M. Yang, F. Yuan, G. Wu, Y. Wei, X. Huang and Y. Zhu: Heterogeneous lamella structure unites ultrafine-grain strength with coarse-grain ductility *Proceedings of the National Academy of Sciences.* **112**(47), 14501 (2015).
- 8. B.Q. Han, Z. Lee, D. Witkin, S. Nutt and E.J. Lavernia: Deformation behavior of bimodal nanostructured 5083 Al alloys *Metallurgical and Materials Transactions A: Physical Metallurgy and Materials Science.* **36**(4), 957 (2005).
- 9. C. Sawangrat, S. Kato, D. Orlov and K. Ameyama: Harmonic-structured copper: performance and proof of fabrication concept based on severe plastic deformation of powders *Journal of Materials Science*. **49**(19), 6579 (2014).
- 10. X. Ma, C. Huang, J. Moering, M. Ruppert, H.W. Höppel, M. Göken, J. Narayan and Y. Zhu: Mechanical properties of copper/bronze laminates: Role of interfaces *Acta Materialia*. **116**, 43 (2016).
- 11. Y. Zhao, T. Topping, J.F. Bingert, J.J. Thornton, A.M. Dangelewicz, Y. Li, W. Liu, Y. Zhu, Y. Zhou and E.J. Lavernia: High Tensile Ductility and Strength in Bulk Nanostructured Nickel *Advanced Materials*. **20**(16), 3028 (2008).
- 12. Y. Wang, M. Chen, F. Zhou and E. Ma: High tensile ductility in a nanostructured metal *Nature*. **419**(6910), 912 (2002).
- 13. B.Q. Han, J.Y. Huang, Y.T. Zhu and E.J. Lavernia: Strain rate dependence of properties of cryomilled bimodal 5083 Al alloys *Acta Materialia*. **54**(11), 3015 (2006).
- 14. X. Wu, F. Yuan, M. Yang, P. Jiang, C. Zhang, L. Chen, Y. Wei and E. Ma: Nanodomained nickel unite nanocrystal strength with coarse-grain ductility *Scientific Reports.* 5, (2015).
- 15. S. Huang, J. Wang, N. Li, J. Zhang and C. Zhou: Atomistic simulations of plasticity in heterogeneous nanocrystalline Ni lamella *Computational Materials Science*. **141**, 229 (2018).
- 16. S. Huang, J. Wang and C. Zhou: Deformation of Heterogeneous Nanocrystalline Lamella with a Preexisting Crack *JOM*. **70**(1), 60 (2018).

- 17. F. Roters, P. Eisenlohr, L. Hantcherli, D.D. Tjahjanto, T.R. Bieler and D. Raabe: Overview of constitutive laws, kinematics, homogenization and multiscale methods in crystal plasticity finite-element modeling: Theory, experiments, applications *Acta Materialia*. **58**(4), 1152 (2010).
- 18. E.B. Marin and P.R. Dawson: On modelling the elasto-viscoplastic response of metals using polycrystal plasticity *Computer Methods in Applied Mechanics and Engineering*. **165**(1), 1 (1998).
- 19. R. Yuan, I.J. Beyerlein and C. Zhou: Emergence of grain-size effects in nanocrystalline metals from statistical activation of discrete dislocation sources *Acta Materialia*. **90**(0), 169 (2015).
- 20. R. Yuan, I.J. Beyerlein and C. Zhou: Coupled crystal orientation-size effects on the strength of nano crystals *Scientific Reports*. **6**, Accepted (2016).
- 21. A. Foreman: The bowing of a dislocation segment *Philosophical magazine*. **15**(137), 1011 (1967).
- 22. R. Madec, B. Devincre and L. Kubin: From dislocation junctions to forest hardening *Physical review letters.* **89**(25), 255508 (2002).
- 23. J. Li and A. Soh: Modeling of the plastic deformation of nanostructured materials with grain size gradient *International Journal of Plasticity*. **39**, 88 (2012).
- 24. H. Mecking and U. Kocks: Kinetics of flow and strain-hardening *Acta Metallurgica*. **29**(11), 1865 (1981).
- 25. A. Ma, F. Roters and D. Raabe: A dislocation density based constitutive model for crystal plasticity FEM including geometrically necessary dislocations *Acta Materialia*. **54**(8), 2169 (2006).
- 26. M. Jahedi, M. Ardeljan, I.J. Beyerlein, M.H. Paydar and M. Knezevic: Enhancement of orientation gradients during simple shear deformation by application of simple compression *Journal of Applied Physics*. **117**(21), 214309 (2015).
- 27. R. Zhu, J. Zhou, H. Jiang and D. Zhang: Evolution of shear banding in fully dense nanocrystalline Ni sheet *Mechanics of Materials*. **51**, 29 (2012).
- 28. F. Ebrahimi, G. Bourne, M.S. Kelly and T. Matthews: Mechanical properties of nanocrystalline nickel produced by electrodeposition *Nanostructured materials*. **11**(3), 343 (1999).
- 29. E. Ma and T. Zhu: Towards strength–ductility synergy through the design of heterogeneous nanostructures in metals *Materials Today*. **20**(6), 323 (2017).
- 30. L. Li, P.M. Anderson, M.-G. Lee, E. Bitzek, P. Derlet and H. Van Swygenhoven: The stress–strain response of nanocrystalline metals: a quantized crystal plasticity approach *Acta Materialia*. **57**(3), 812 (2009).
- 31. S.-H. Choi, E.-Y. Kim, W. Woo, S. Han and J. Kwak: The effect of crystallographic orientation on the micromechanical deformation and failure behaviors of DP980 steel during uniaxial tension *International Journal of Plasticity.* **45**, 85 (2013).
- 32. M.A. Meyers and K.K. Chawla: Mechanical behavior of materials, (2009).
- 33. T. Rupert, D. Gianola, Y. Gan and K. Hemker: Experimental observations of stress-driven grain boundary migration *Science*. **326**(5960), 1686 (2009).
- 34. S. Huang, I.J. Beyerlein and C. Zhou: Nanograin size effects on the strength of biphase nanolayered composites *Scientific Reports*. **7**(1), 11251 (2017).

- 35. C. Brandl, S. Tiwari, P.M. Derlet and H. Van Swygenhoven: Athermal critical stresses for dislocation propagation in nanocrystalline aluminium *Philosophical Magazine*. **90**(7-8), 977 (2010).
- 36. S. Huang and C. Zhou: Modeling and simulation of nanoindentation *JOM*. **69**(11), 2256 (2017).
- 37. C. Zhou, I.J. Beyerlein and R. LeSar: Plastic deformation mechanisms of fcc single crystals at small scales *Acta Materialia*. **59**(20), 7673 (2011).
- 38. C. Zhou, S.B. Biner and R. LeSar: Discrete dislocation dynamics simulations of plasticity at small scales *Acta Materialia*. **58**(5), 1565 (2010).

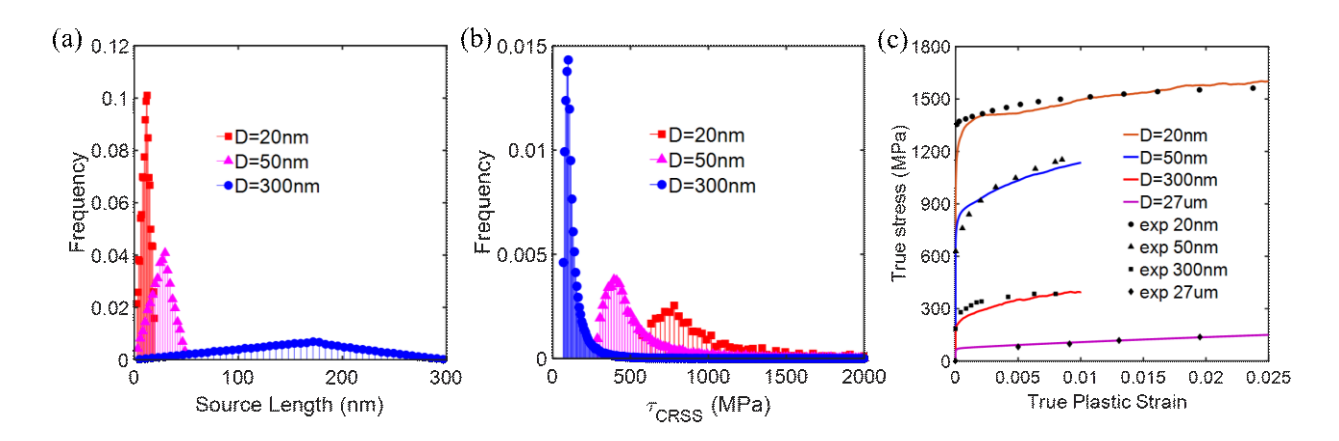


Figure 1. Probability density distributions of (a) dislocation source lengths and (b) τ_{CRSS} for different grain size; (c) predicted stress-strain curves for polycrystalline Ni of grain size 20nm 27 , 50nm 28 , 300nm 28 , and 27 μ m 29 compared with experimental results.

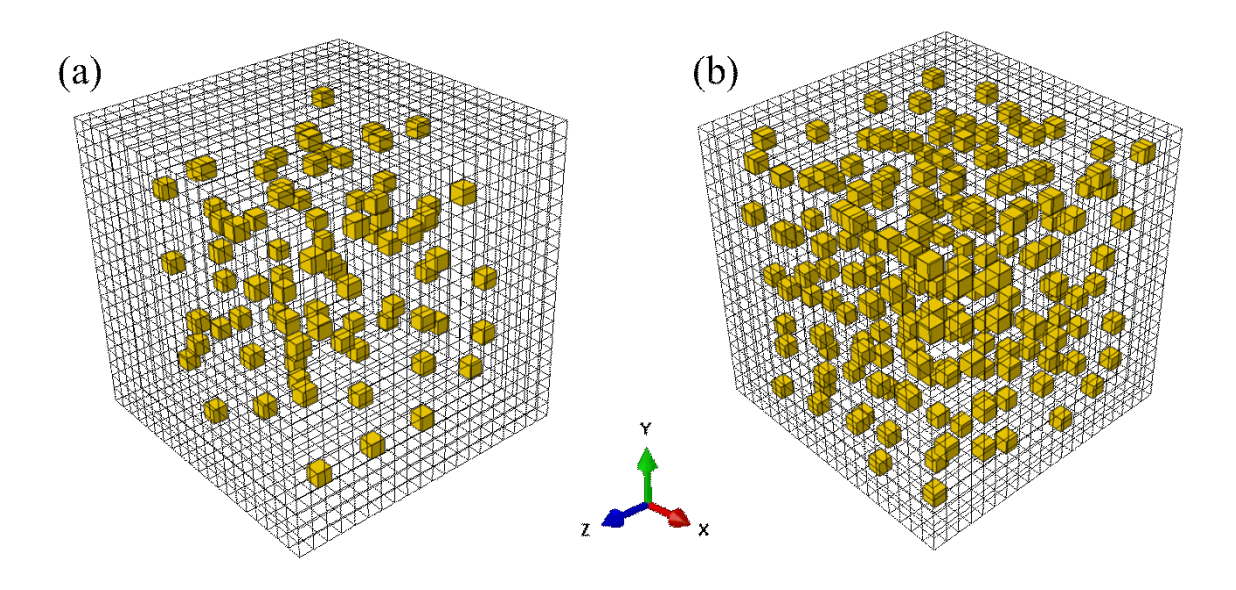


Figure 2. 3D model of nanodomained (ND) structure comprising embedded nanograins (orange) and a single coarse grain (transparent). (a) 1% nano grains (NGs); (b) 2.5% NGs.

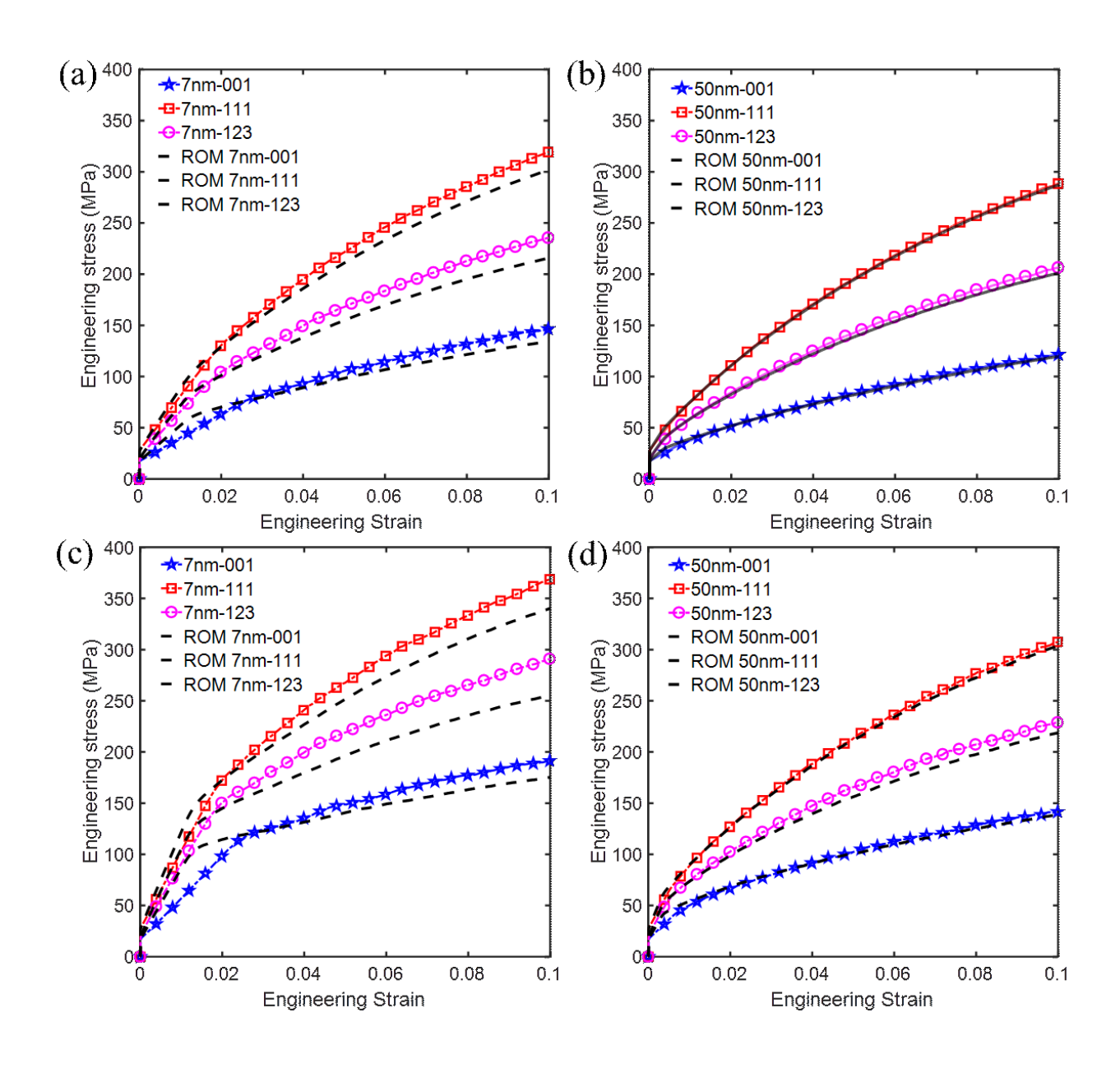


Figure 3. Comparison of CPFE calculated stress-strain curves with ROM curves: (a) 1% of 7nm NGs, (b) 1% of 50nm NGs, (c) 2.5% of 7nm NGs, (d) 2.5% of 50nm NGs.

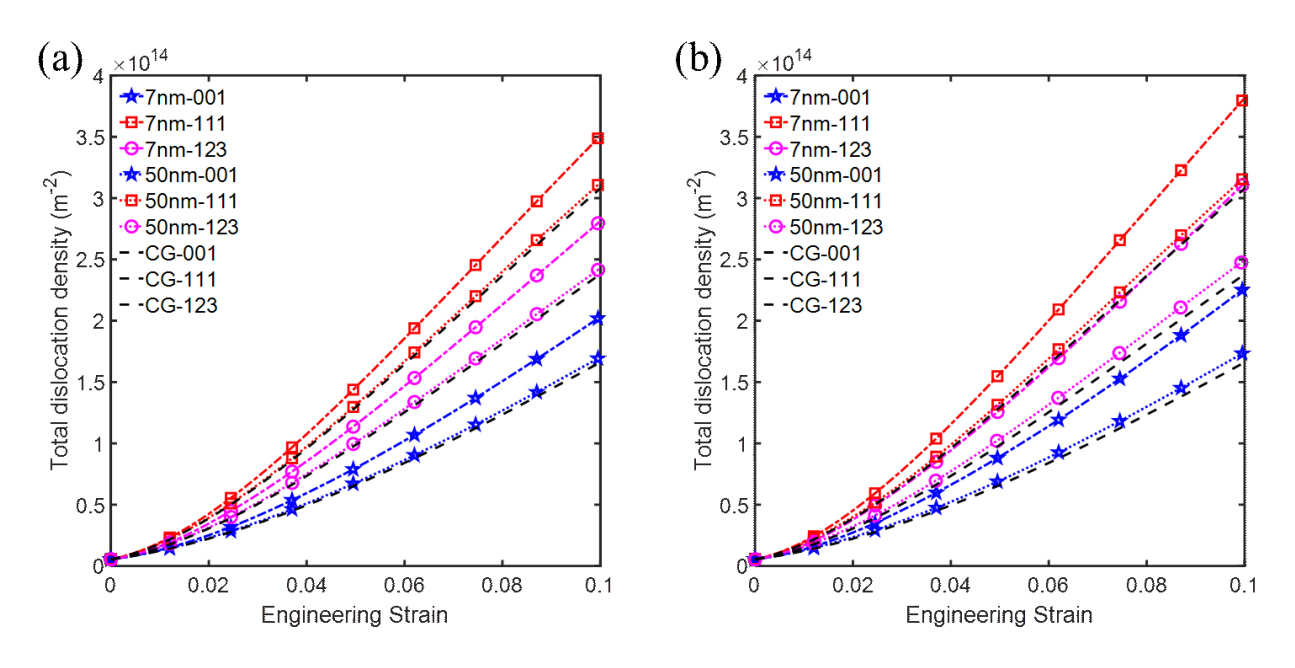


Figure 4. Evolution of the total dislocation density: (a) 1% NGs, (b) 2.5% NGs.

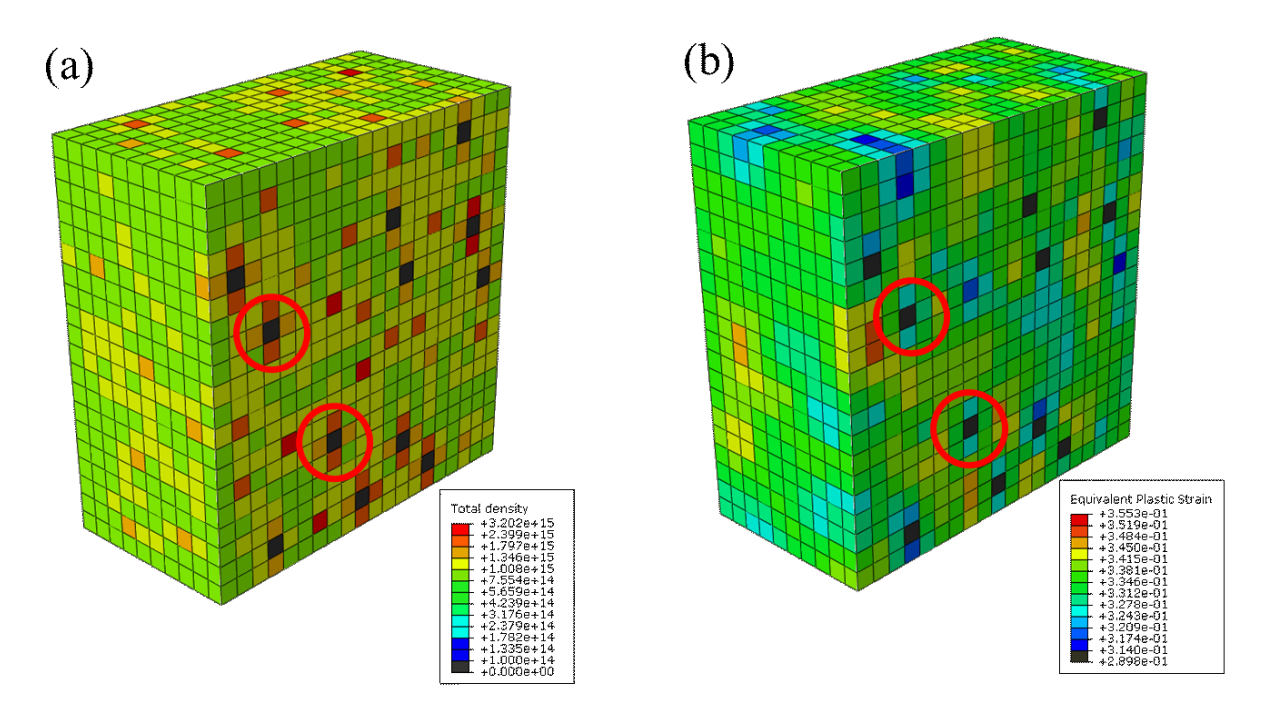


Figure 5. Distribution of (a) the total dislocation density and (b) the equivalent plastic strain within the sample with 2.5% 7nm NGs at 10% strain. (Black elements represent nano grains embedded in the coarse grain.)

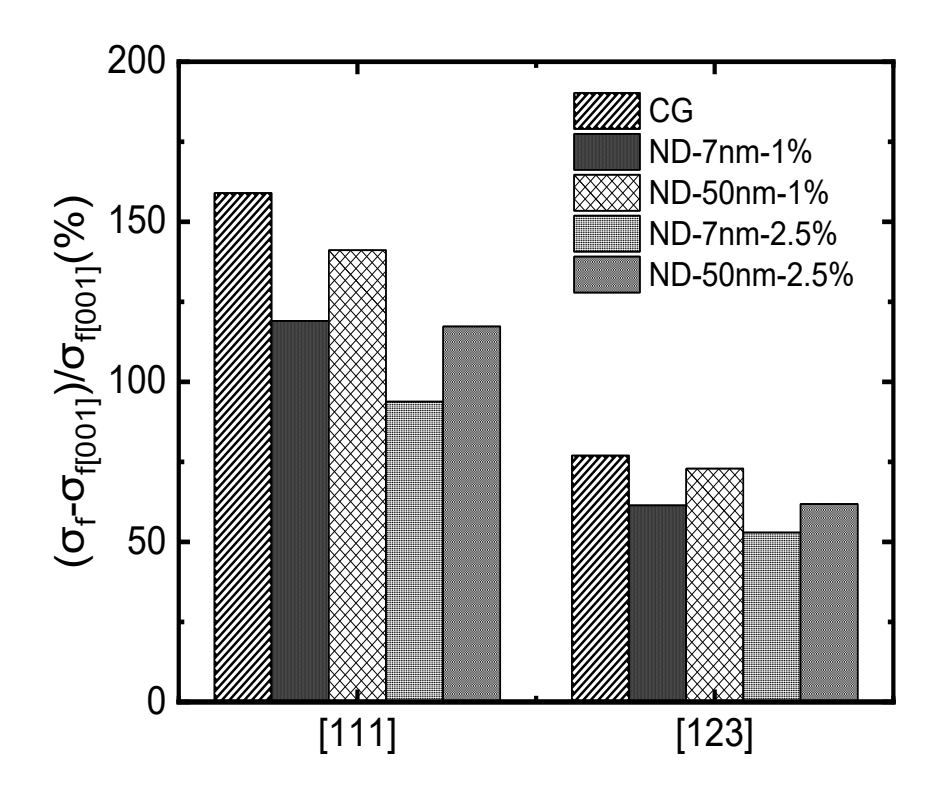


Figure 6. Comparison of the anisotropy of the strength at 0.1 strain for different cases.